High-pressure reactively sputtered Hf O 2 : Composition, morphology, and optical properties

M. Toledano-Luque, E. San Andrés, A. del Prado, I. Mártil, M. L. Lucía, G. González-Díaz, F. L. Martínez, W. Bohne, J. Röhrich, and E. Strub

Citation: Journal of Applied Physics **102**, 044106 (2007); doi: 10.1063/1.2769959
View online: http://dx.doi.org/10.1063/1.2769959
View Table of Contents: http://scitation.aip.org/content/aip/journal/jap/102/4?ver=pdfcov
Published by the AIP Publishing

High-pressure reactively sputtered HfO_2: Composition, morphology, and optical properties

M. Toledano-Luque,[a] E. San Andrés, A. del Prado, I. Mártil, M. L. Lucía, and G. González-Díaz
Dpto. de Física Aplicada III, Fac. Ciencias Físicas, Universidad Complutense de Madrid, Ciudad Universitaria, E-28040 Madrid, Spain

F. L. Martínez
Dpto. de Electrónica y Tecnología de Computadoras, Universidad Politécnica de Cartagena, E-30202 Cartagena, Spain

W. Bohne, J. Röhrich, and E. Strub
Hahn-Meitner-Institut Berlin, Abteilung SF4, D-14109 Berlin, Germany

(Received 14 April 2007; accepted 5 July 2007; published online 22 August 2007)

Hafnium oxide films were deposited by high pressure reactive sputtering using different deposition pressures and times. The composition, morphology, and optical properties of the films, together with the sputtering process growth kinetics were investigated using heavy ion elastic recoil detection analysis, Fourier transform infrared spectroscopy, ultraviolet-visible-near infrared spectroscopy, x-ray diffraction, and transmission electron microscopy. The films showed a monoclinic polycrystalline structure, with a grain size depending on the deposition pressure. All films were slightly oxygen rich with respect to stoichiometric HfO_2 and presented a significant amount of hydrogen (up to 6 at. %), which is attributed to the high affinity for moisture of the HfO_2 films. The absorption coefficient was fitted to the Tauc law, obtaining a band gap value of 5.54 eV. It was found that the growth rate of the HfO_2 films depends on the deposition pressure (P) as $P^{-1.75}$. This dependence is explained by a diffusion model of the thermalized atoms in high-pressure sputtering. Additionally, the formation of an interfacial silicon oxide layer when the films were grown on silicon was observed, with a minimum thickness for deposition pressures around 1.2 mbars. This interfacial layer was formed mainly during the initial stages of the deposition process, with only a slight increase in thickness afterwards. These results are explained by the oxidizing action of the oxygen plasma and the diffusion of oxygen radicals and hydroxyl groups through the polycrystalline HfO_2 film. Finally, the dielectric properties of the HfO_2/SiO_2 stacks were studied by means of conductance and capacitance measurements on $Al/HfO_2/SiO_2/Si$ devices as a function of gate voltage and ac frequency signal. © *2007 American Institute of Physics*. [DOI: 10.1063/1.2769959]

I. INTRODUCTION

Thin films of transition metal oxides, especially HfO_2, have been extensively studied due to their broad range of applications. The high values of their dielectric constant make them suitable candidates for replacing the silicon oxide and oxynitride insulating film in field effect transistors[1] and dynamic random access memories.[2] Due to the large bang gap and high refractive index, HfO_2 is also an interesting material for optical applications. HfO_2 is regularly used as optical coating for astronomical charge coupled devices (CCDs),[3] as antireflective multilayer coating for night vision devices, and for IR optical devices.[4] Moreover, HfO_2 is used in pH, Na^+, K^+, and H^+ chemical sensors,[5] and in physical sensors for on chip temperature detection.[6] The application of high-k materials in bioelectronics has also been studied due to the efficient capacitive interaction of silicon chips and living cells.[7] Finally, HfO_2 is an interesting protective coating for applications in contact with harsh environments due to the high chemical inertness.[8]

In this work, the properties of HfO_2 thin films grown by high-pressure reactive sputtering[9] (HPRS) are studied. This nonconventional deposition method works at chamber pressures in the order of 1 mbar, which is about two or three orders of magnitude higher than in conventional sputtering systems. Due to the high pressure, the mean free path of the plasma species is significantly shorter (about 0.05 mm),[10] so that the plasma region is confined in the neighborhood of the target. Besides, the particles emitted by the target collide with the gaseous medium, losing energy, thermalizing within a short distance of the cathode, and then reaching the substrate by means of a pure diffusion process. Therefore, this deposition method prevents the impact of high-energy species on the substrate and on the growing film, greatly reducing the damage to the interface and the film itself. Another advantage of this technique is the possibility of working with several targets, allowing the fabrication of multilayered structures or compounds. This technique has been successfully used to grow high-T_c superconductor films,[11] titanium oxide (TiO_2) films,[12] and multilayer buffers for high-T_c superconductor devices[13] using a multitarget system.

In this work, the physical properties and growth kinetics

[a]Author to whom correspondence should be addressed; FAX: +34 91 394 5196; electronic mail: mtluque@fis.ucm.es

of high-pressure reactively sputtered HfO_2 are studied as a function of deposition pressure and time. Also, the possible applications in the different fields presented in this section are analyzed. Results of measurements on TiO_2 films[12] deposited with the same equipment are discussed for comparison.

II. EXPERIMENT

The details of the HPRS system used to grow the HfO_2 films were given elsewhere.[12,14] A commercial HfO_2 target with nominal purity of 99.95% (except, Zr) and a diameter of 4.5 cm was used. O_2 was used as reactive gas. It is emphasized that the only elements purposefully introduced in the process are those composing the deposited film, i.e., Hf and O. Therefore, the purity of the sputtered films can be controlled by the purity of the target, in contrast to other deposition techniques such as chemical vapor deposition (CVD) or atomic layer deposition (ALD) where the impurity incorporation in the deposited films is always a cause of concern.

Two series of samples were fabricated. In the first one, the depositions were performed during 180 min with pressures ranging from 0.8 to 1.6 mbars. In the second series, the deposition pressure was kept constant at 1.2 mbars, while the deposition time was varied between 2 and 150 min. In both series, the radio frequency power was 60 W, the substrate temperature was 200 °C, and the target to substrate holder distance was 2.5 cm.

The substrate for the HfO_2 growth was selected according to the characterization technique. For the optical measurements, UV-grade quartz (silica), whose transparency range extends down to 190 nm covering the absorption edge of hafnium oxide, was used. The samples for the other techniques were prepared on single side polished *n*-Si (100) wafers with a resistivity of 4.6–5.0 Ω cm or for infrared spectroscopy on double side polished *p*-Si (111) wafers with high resistivity (80 Ω cm). The wafers were cut into 1×1 cm^2 pieces and subjected to a standard RCA cleaning method.[15] Just before introduction into the chamber the native oxide was removed by immersion in diluted HF (50:1) for 30 s.

The bonding structure was studied by Fourier transform infrared spectroscopy (FTIR) in the 150–4000 cm^{-1} range using a Nicolet Magna-IR 750 series II spectrometer working in transmission mode at normal incidence. The composition of the films was measured by heavy ion elastic recoil detection analysis (HI-ERDA) using 350 MeV Au ions. The different species were identified by the time-of-flight technique.[16,17] The ion fluence was in the order of 10^{12} atoms/cm^2, which is low enough to minimize preferential effusion effects of light atoms, which take place at higher ion fluences.[18] This technique provides the absolute atomic concentration of every species present in the film and the total atomic area density (atoms/cm^2), without needing calibration standards. Transmittance (T) and reflectance (R) spectra were measured in the ultraviolet–visible–near infrared range (UV-Visible-NIR) by means of a Perkin-Elmer Lambda 9 spectrometer. The optical constants were extracted from the spectra following the procedure of Hernández-Rojas *et al.*[19] The nature and the value of the band gap (E_G) were determined from a fit of the data according to the Tauc law.[20] X-ray diffraction (XRD) was performed to study the crystallinity of the films using a Philips XPERT diffractometer with Cu $K\alpha$ radiation in θ-2θ configuration. The HfO_2 peak near $2\theta=28.35°$ was used to estimate the grain size by means of the Scherrer equation.[21] The film and interface morphology and thickness were investigated by transmission electron microscopy (TEM) using a JEOL JEM-2000FX microscope operated at 200 keV. Finally, metal oxide semiconductor (MOS) devices were fabricated by e-beam evaporation of Al electrodes in order to evaluate the dielectrical properties of the films. Capacitance and conductance measurements as a function of voltage and frequency were carried out by means of an Agilent 4294A impedance analyzer. The density of interfacial traps (D_{it}) was evaluated by means of the following equations:[22]

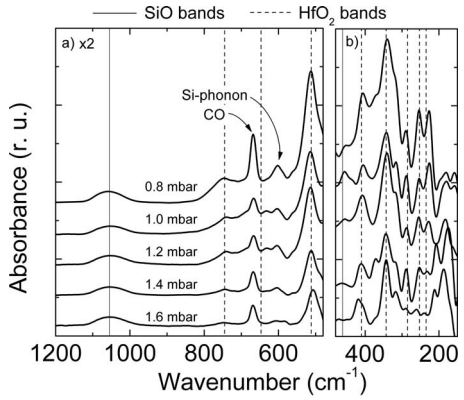

FIG. 1. FTIR spectra of samples deposited at different pressures, divided into two frequency regions: (a) 1200–475 cm^{-1} and (b) 475–150 cm^{-1}. The main absorption bands corresponding to monoclinic HfO_2 and SiO_2 are also shown.

$$D_{it}=\frac{G_P/\omega}{0.4qA}, \tag{1}$$

$$\frac{G_P}{\omega}=\frac{\omega C_{ox}^2 G_m}{G_m^2+\omega^2(C_{ox}-C_m)^2}, \tag{2}$$

where G_P is the maximum of the peak of the equivalent parallel silicon conductance calculated from the measured capacitance (C_m), conductance (G_m), and oxide capacitance (C_{ox}). The oxide capacitance (C_{ox}) was determined from the admittance as a function of frequency in strong accumulation. The C-V and G-V measurements were performed at a frequency of 50 kHz, for which the maximum value of G_P/ω were obtained.

Finally, the frequency dispersion of the calculated relative dielectric permittivity of HfO_2 was studied in the frequency range from 40 Hz to 200 kHz.

III. RESULTS AND DISCUSSION

A. FTIR analysis

The bond structure of the films was studied by FTIR. Figure 1 shows the FTIR spectra of the samples deposited at different deposition pressures. Note that each spectrum is divided into two frequency ranges corresponding to the de-

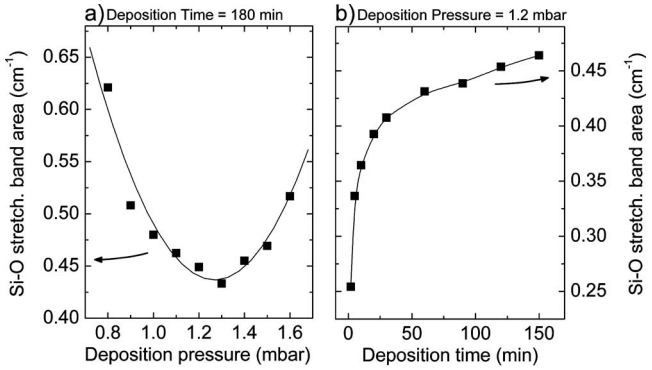

FIG. 2. Si–O stretching band area of the FTIR spectra as a function of (a) the deposition pressure (at constant deposition time of 180 min) and (b) the deposition time (at constant pressure of 1.2 mbars).

tectors used in the measurement. These IR spectra were measured between 150 and 4000 cm^{-1}, but the only significant spectral features were found in the 150–1200 cm^{-1} range, which is shown in Fig. 1.

The peak observed at 670 cm^{-1} is related to CO present in the background, and the band around 610 cm^{-1} is attributed to the absorption of a strong Si phonon.[23] Therefore, neither of them will be further discussed.

Several bands associated with HfO_2 are observed at 410, 343, 285, 253, and 235 cm^{-1} in the far IR, and at 748 and 512 cm^{-1} in the mid-IR. The position of these bands are in agreement with the findings for monoclinic HfO_2.[24] The peaks situated in the mid-IR have been reported previously and assigned to the transverse optical (TO) phonon modes.[23] A decrease of the height and area of the strong absorption bands is observed when deposition pressure is increased, suggesting a decrease of the HfO_2 thickness and deposition rate (keeping in mind that the deposition time was kept constant).

Two bands at 1056 and 461 cm^{-1} associated with silicon oxide are also observed in Fig. 1. The band located at around 461 cm^{-1} corresponds to the bending mode of the Si–O–Si bond, while the band located at 1056 cm^{-1} is characteristic of an asymmetric stretching vibration of the SiO_4 unit in strained SiO_2.[25] We attribute these bands to the formation of an interfacial SiO_2 layer between the HfO_2 film and the Si substrate during the deposition. The presence of silicon suboxides near the Si/SiO_2 interface[25] and/or that the Hf–O bonds are longer than the Si–O bonds[26] may be responsible for the strain in this layer. Figure 2(a) shows the area of the Si–O stretching band as a function of deposition pressure. The band area is proportional to the concentration of bonds associated with that band. A minimum is observed for the films deposited at around 1.2–1.3 mbars, suggesting a minimum in the thickness of the SiO_2 interfacial layer. To further study the growth kinetics of this interfacial layer, other series of nine samples was deposited, keeping the deposition pressure constant at 1.2 mbars and varying the deposition time from 2 to 150 min. A shift of the band to lower wave numbers down to 1049 cm^{-1}, together with a decrease of the area, was observed as the deposition time was reduced. Figure 2(b) shows the area of the asymmetric stretching band of the SiO_4 unit as a function of deposition time. A nonlinear

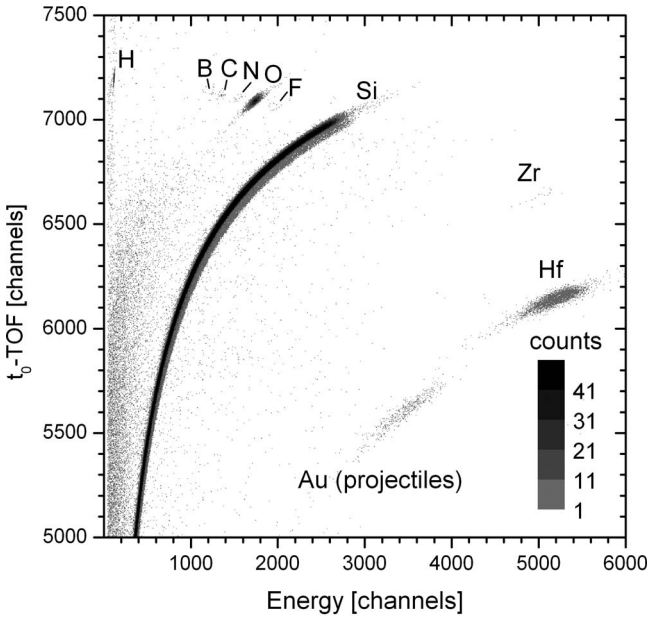

FIG. 3. Scatterplot of the inverse time-of-flight (t_0-TOF) of the ions as a function of their energy for a sample deposited at 1.2 mbars on Si.

dependence is observed, with a great increase of the area for deposition times up to 30 min and a slight increase for longer deposition times. This behavior indicates that the SiO_2 interfacial layer grows mainly during the early stages of deposition, reducing its growth rate as the thickness of the hafnium oxide layer increases.

B. HI-ERDA analysis

Figure 3 presents a representative scatterplot of time-of-flight of the elements as a function of their energy obtained by HI-ERDA for the HfO_2 film deposited at 1.2 mbars. Due to the limited depth resolution of the HI-ERDA analysis and the low thickness of the interfacial layer, it is difficult to separate the oxygen coming from the HfO_2 film and from the SiO_2 film. Therefore, for the calculation of the concentration of each species in the HfO_2 film, the thickness of the SiO_2 obtained by TEM measurements were taken into account. The calculations were performed by simultaneous fitting of the energy spectra of all contributing elements using the simulation code SIMNRA.[27] Table I summarizes the obtained atomic concentrations of the detected elements, as well as the oxygen to hafnium ratios. All samples were slightly oxygen rich ([O]/[Hf]>2) and contained significant amounts of H (up to 6 at. %). Small concentrations of other elements (Zr, F, N, B, and C) were also found. The origin of these elements is now analyzed. Zirconium comes from the HfO_2 target itself. Zr is a usual impurity in the hafnium because they are difficult to separate. Fluorine may originate from the RCA cleaning process whereas nitrogen may have been incorporated during the deposition due to the residual gas in the chamber. Hydrogen is an element difficult to evacuate from the chamber and it may react with the oxygen to form hydroxyl groups thus incorporating in the growing film. Therefore, the hydrogen and the oxygen excess in the HfO_2 films may be attributed to the affinity for the adsorption of hydroxyl (–OH) groups or moisture of the HfO_2 films.[28] In a

TABLE I. Composition obtained by HI-ERDA for samples deposited at different deposition pressures. The uncertainty of the [O]/[Hf] ratio is about 3%.

p (mbar)	0.8	0.9	1.0	1.1	1.2	1.4	1.6
Hf (at. %)	30.7	30.1	30.4	29.4	28.5	29.4	30.6
O (at. %)	65.0	62.5	61.4	63.6	62.6	63.7	62.3
H (at. %)	3.2	5.5	5.1	4.0	5.3	6.0	6.0
B, C, N, F, Zr (at. %)	1.1	1.9	3.1	3.0	3.6	0.9	1.1
[O]/[Hf]	2.1	2.1	2.0	2.2	2.2	2.2	2.0

previous study concerning the growth of TiO_2 films using the same HPRS system and the same deposition procedure (same sputtering parameters and Si-substrate cleaning),[12] similar concentrations of F, B, C, and N impurities were found. However, the H concentration was lower than 1%. This supports the assumption that the small amounts of F, B, C, and N are related to the cleaning or the deposition technique. Nevertheless, the H excess in the HfO_2 films is associated with high affinity for moisture of this material.

The density of the HfO_2 films was obtained from the HI-ERDA area densities concentrations (atoms/cm^2) and the thickness measured by TEM. The obtained values are shown in Fig. 4 as a function of deposition pressure. The error bars are about 10% and include the uncertainties due to the determination of the HfO_2 and the SiO_2 thicknesses by TEM as well as the counting statistics in the HI-ERDA procedure. The theoretical value for HfO_2 bulk density is 10.1 g/cm^3, determined from the unit cell parameters of the monoclinic phase. Density values slightly higher than the theoretical value, but within the uncertainty of the technique, were obtained for the samples deposited at 0.8 and 1.6 mbars. Lower densities were measured for the films deposited at intermediate pressure. The lowest value was obtained for the sample deposited at 1.0 mbar. As it will be discussed later, for this intermediate range of pressures the highest grain sizes were observed, also shown in Fig. 2, suggesting a relationship between the density of the films and the grain size.

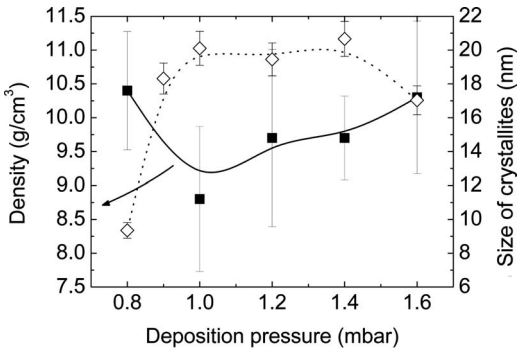

FIG. 4. HfO_2 mass density (left) and mean grain size (right) as a function of the deposition pressure. The lines are drawn as a guide to the eyes.

C. UV-visible-*NIR* analysis

The transmittance and reflectance spectra in the ultraviolet-visible-near infrared region were measured in order to determine the optical properties of a representative film deposited at 1.2 mbars. The complex refractive index was obtained by means of numerical analysis, taking into account the scattering of the light caused by surface roughness. The details of the calculations are given elsewhere.[19] Figure 5(a) shows the real part of the refractive index as a function of the wavelength λ. These values are slightly lower than the HfO_2 bulk value (n=2.08 at 600 nm).[29]

The absorption coefficient α was calculated from the imaginary part k of the refractive index as $\alpha=4\pi k/\lambda$. The absorption edge as a function of photon energy is determined by the nature and value of the band gap. Thin films with indirect band gaps usually follow the Tauc law[20]

$$(\alpha h\nu)^{1/2} = B_{\text{Tauc}}(h\nu - E_G). \tag{3}$$

Figure 5(b) shows the plot of $(\alpha h\nu)^{1/2}$ as a function of $h\nu$. The Tauc parameter B_{Tauc} and the band gap value are obtained from the slope of the linear region and its intersection with $(\alpha h\nu)^{1/2}=0$, respectively. A band gap value of 5.54 eV was obtained from the fit, in agreement with other reports.[1] The values obtained for both refractive index and band gap energy indicate that the films are transparent down to 223 nm (UV range) and therefore HfO_2 films present a potential use as a transparent coating.

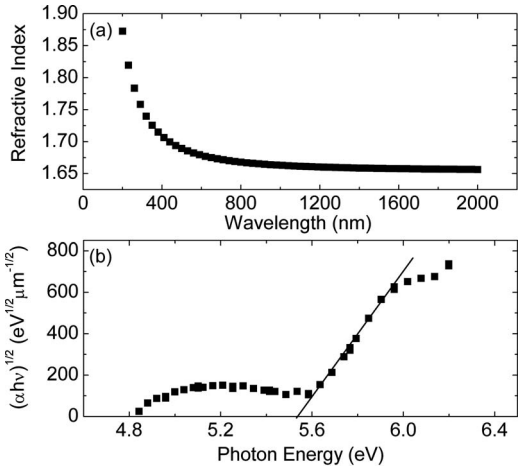

FIG. 5. (a) Refractive index and (b) $(\alpha h\nu)^{1/2}$ as a function of $h\nu$ for HfO_2 deposited at 1.2 mbars. The optical gap is obtained by fitting the absorption edge to the Tauc law. A linear fit is shown.

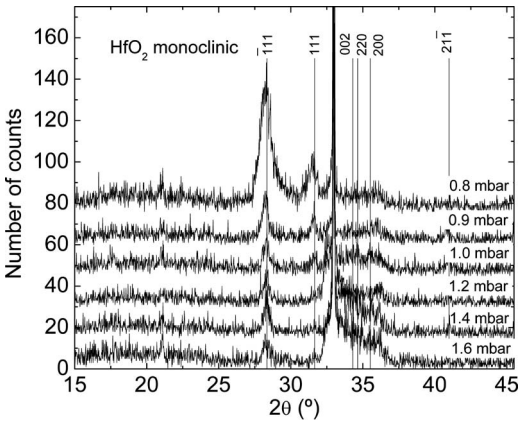

FIG. 6. XRD diagrams from samples deposited at different pressures. The main peaks are labeled according to the pattern of monoclinic HfO_2.

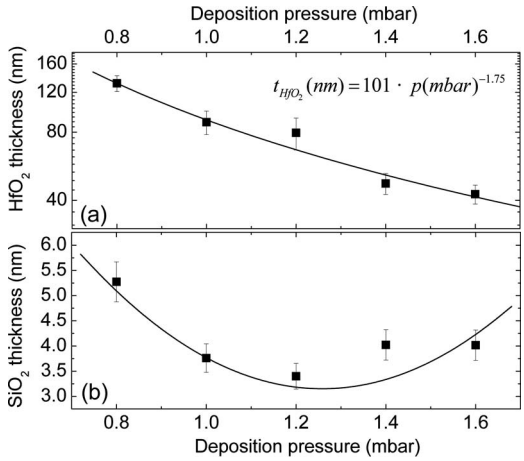

FIG. 7. Thickness of the HfO_2 films (top) and the SiO_2 interfacial layers (bottom) as a function of the deposition pressure. The fit between HfO_2 thickness and deposition pressure is shown. The line in (b) is a guide to the eyes.

D. XRD analysis

Figure 6 shows the XRD spectra of the HfO_2 films deposited at different pressures and the position of several reflections associated with the monoclinic phase of HfO_2.[30] The main peak of this phase is located at 28.35° and corresponds to the $\bar{1}11$ reflection. Secondary peaks of this phase are also visible. Thus, the XRD measurements support a polycrystalline structure of the HfO_2 films, and the peak positions confirm a monoclinic phase. The average grain size, which is shown in Fig. 4, was estimated according to the Scherrer equation[21] from the full width at half maximum (FWHM) of the $\bar{1}11$ reflection peak, obtained by fitting the spectra by Gaussian shaped lines. The peak intensity of the $\bar{1}11$ monoclinic HfO_2 feature decreases with increasing deposition pressure. The sample deposited at 0.8 mbar presents the smallest grain size (~8 nm), whereas the samples deposited between 0.9 and 1.4 mbars have a roughly constant grain size (~20 nm). Finally, at 1.6 mbars the grain size decreases with respect to intermediate deposition pressures (~16 nm). As shown above, the lowest densities of the films are related to the largest grain sizes, probably due to void space between crystallites. In the sensor applications area where layers with a very low chemical reactivity are necessary, hafnium oxide is a promising candidate. In this field a high mass density with a structure of small crystallites is required.[8] These characteristics are obtained when the HfO_2 films are grown at the lowest pressures studied, indicating that HPRS HfO_2 can be used in that field.

E. TEM analysis

The cross-sectional TEM images of HfO_2 films deposited at different pressures were obtained to confirm the HPRS HfO_2/SiO_2 stacked structure. HfO_2 polycrystalline layers were observed on top of thinner amorphous films. The amorphous films were identified as SiO_2, in agreement with the FTIR results. The electron diffraction patterns of the HfO_2 films could be explained by a polycrystalline monoclinic phase, further supporting the FTIR and XRD results. The thickness of the HfO_2 films determined from the TEM images are shown in Fig. 7(a) as a function of deposition pressure. A decrease of the HfO_2 thickness with increasing deposition pressure is observed, as previously suggested by the FTIR results. This can be explained as follows. In our HPRS system, the mean free path length of the working gas varies inversely with pressure, covering values from 0.04 to 0.08 mm for deposition pressures from 1.6 to 0.8 mbar, respectively.[31] The average energy of the sputtered particles is less than 10 eV.[32] The average fractional energy lost (final energy/initial energy) may be estimated from the binary collisions theory.[10] In the case of sputtered hafnium slowing down in collisions with O_2 molecules, the average fractional energy lost is about 0.75. Therefore, the sputtered hafnium is thermalized after 20 collisions, travelling a maximum distance of 0.16 and 0.08 cm for a deposition pressure of 0.8 and 1.6 mbars, respectively. The thermalization distance of the sputtered atoms is much shorter than the target to substrate distance (2.5 cm) and therefore they are transported to the substrate by a diffusion process. Then the thermalization distance of the sputtered particles decreases accordingly with pressure and the spatial profile of the thermalizated particles approaches the cathode. The sputtered particles have to diffuse a longer distance to reach the substrate with increasing pressure thus decreasing the growth rate. Moreover, the transport of thermalized particles is less efficient with increasing pressure because the diffusion coefficient is reduced. The relationship between the thickness and the pressure can be fitted by

$$t_{\mathrm{HfO_2}}(\mathrm{nm}) = 101 p(\mathrm{mbar})^{-1.75}. \quad (4)$$

Znamenski *et al.*[33] found a similar dependency with pressure for the atomic flux reaching the substrate j_s (calculated from the thickness of the film) for high-pressure magnetron sputtering ($j_s \approx P^{-2}$) and proposed a diffusion model to explain the transport of the thermalized atoms. Our results are consistent with the proposed model.

Similarly, the same approximations are applied to the reflected atoms on the target. The maximum travelling distance of these nonthermalized particles is around 0.27 cm when the initial energy is 500 eV. However, a heating of the substrate is observed during the deposition. Due to the short

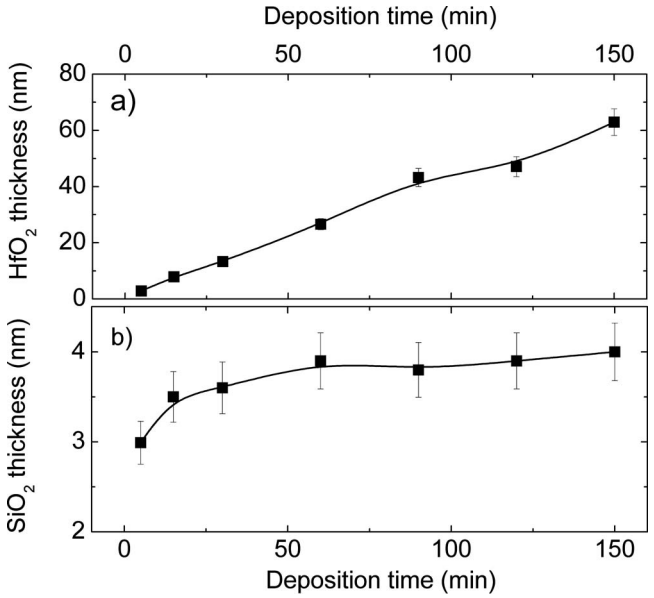

FIG. 8. Thickness of the HfO_2 film (top) and the SiO_2 interfacial layer (bottom) as a function of the deposition time. The lines are guide to the eyes.

thermalization lengths of the sputtered and reflected particles, the energy deposited in the substrate may only come from the secondary electrons, which may promote the polycrystalline growth of the films.

Figure 7(b) shows the thickness of the interfacial SiO_2 layer as a function of deposition pressure. A minimum is observed for pressures around 1.2 mbars, in agreement with the FTIR results for the area of the SiO_2 stretching band [see Fig. 2(a)]. To further investigate the growth mechanism, TEM measurements were performed in a series of seven samples deposited at a constant pressure of 1.2 mbars, with deposition times ranging from 5 to 150 min. Figure 8 shows the SiO_2 and HfO_2 thicknesses derived from these measurements as a function of deposition time. The HfO_2 thickness is directly proportional to deposition time, indicating a constant deposition rate, whereas the SiO_2 layer grows mainly in the initial 30 min and then remains roughly constant, as FTIR measurements suggested [see Fig. 2(b)].

The kinetics of the formation of the interfacial SiO_2 may be explained by two different mechanisms taking place at different stages of the deposition process. At the beginning of the deposition, the high growth rate of SiO_2 is due to the oxidation of the silicon surface by the highly reactive oxygen radicals present in the plasma.[34] The necessary energy to dissociate an oxygen molecule is 5.2 eV, close to the energy of the electrons of the discharge.[10] During the glow discharge, the molecular oxygen is converted into atomic oxygen which reacts readily. Additionally, hafnium oxide has a higher heat of formation than SiO_2.[35] Therefore, SiO_2-like bondings are energetically favored over silicidelike bondings at the interface, and the formation of a thin layer of silicon oxide is unavoidable.

As the deposition process advances and the HfO_2 film gets thicker, the subsequent growth of the silicon oxide interfacial layer is limited by the diffusion of oxygen and/or hydroxyl groups. The polycrystalline structure of the hafnium oxide deposited by HPRS allows the oxygen diffusion through the grain boundaries, which are high diffusivity paths.[36] The diffused oxygen atoms reach the silicon substrate, where they react to form silicon oxide. This mechanism leads to a much slower growth rate of SiO_2, which is reduced by the increase of the HfO_2 thickness.

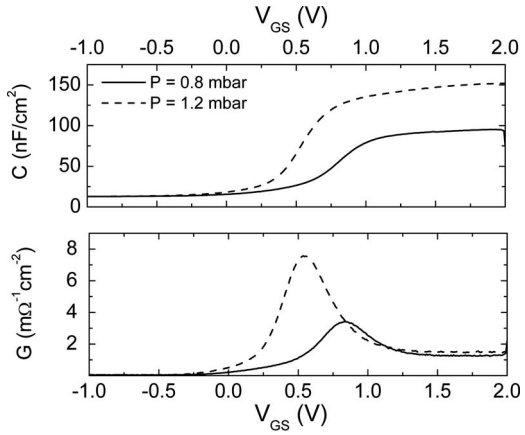

FIG. 9. Capacitance (C) and conductance (G) per unit area (cm^{-2}) as a function of gate voltage (V_{GS}) at 50 kHz for the samples deposited at 0.8 mbar (solid line) and 1.2 mbars (dotted line).

The minimum of the SiO_2 thickness observed for pressures around 1.2 mbars by FTIR and TEM can be explained by considering the influence of deposition pressure on the two mechanisms discussed above. At low pressure the oxidation process that takes place in the initial stages is more effective, because the mean free path of the oxygen radicals in the plasma is longer than at higher pressures, so the plasma volume extends further away from the target and closer to the substrate. As a consequence, the initial oxidation process is faster at low pressure and slows down as the pressure is increased. However, as the HfO_2 film starts to grow, the oxygen radicals that continue the oxidation of the interface have to permeate through the growing HfO_2 film. Hence, the oxidation velocity becomes dependent on the oxygen diffusion rate and the thickness of the HfO_2 film. As the pressure is increased, the oxygen diffusion rate is expected to grow due to the higher oxygen concentration, while the growth rate of the HfO_2 film will become slower [as we saw in Fig. 7(a)], so both factors will contribute to a higher oxidation rate of the interface. As a result of the different influence of deposition pressure on the initial oxidation and on the oxidation through HfO_2, a minimum of interfacial oxide thickness is found for pressures around 1.2 mbars, as shown in Fig. 7(b). The same trend in the SiO_2 thickness as a function of deposition pressure was found previously in TiO_2 samples deposited in the same sputtering system.[12] This points to a SiO_2 thickness dependency on the pressure which is not material related but related to the sputtering system

F. Electrical characterization

Figure 9 shows the C-V and G-V characteristics of the samples deposited at 0.8 and 1.2 mbars. Non zero values of the conductance G are associated with small-signal energy loss. The two sources of small-signal energy loss are series resistance and interface traps.[22] The largest effect of the series resistance takes place in strong accumulation. A series

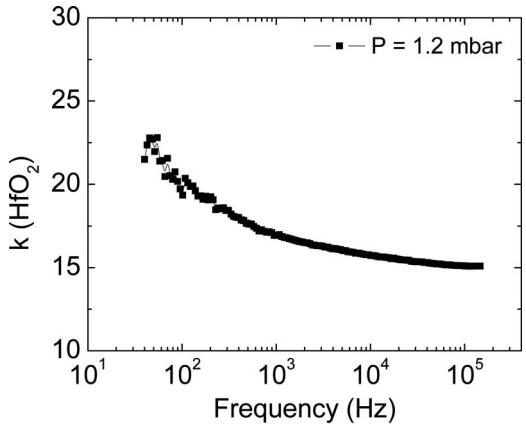

FIG. 10. Calculated HfO_2 dielectric permittivity (k) of the sample deposited at 1.2 mbars.

resistance can cause large distortions in the measurement of the oxide capacitance C_{ox}, and therefore, in the extraction of the density of interfacial traps.[37] The series resistance was calculated from the admittance in strong accumulation and then the measured capacitance and conductance were properly corrected.[22] In depletion, the peak of G is due to the changes in interface level occupancy. The density of interface traps (D_{it}) is determined from the peak of the equivalent parallel silicon conductance G_P extracted from the capacitance and conductance measured in depletion, according to Eqs. (1) and (2). Values of D_{it} of 5×10^{13} and 3×10^{12} eV^{-1} cm^{-2} were obtained for the samples deposited at 0.8 and 1.2 mbars, respectively. These high values are typical for strained silicon oxide, grown far from equilibrium conditions. Postdeposition processes, such as forming gas annealing, would be necessary to release this strain.

The relative dielectric permittivity of the HfO_2 deposited at 1.2 mbars was calculated by modeling the capacitance of the insulator as two capacitances in series, one corresponding to the HfO_2 layer and the other to the SiO_2 interfacial layer. The dielectric permittivity calculated from the measured capacitance in accumulation at 50 kHz, after series resistance correction, was 17. This value is slightly lower than reported values using different deposition techniques.[1] In order to gain insight into the reasons for this smaller k value, we performed a frequency study. Figure 10 shows the calculated dielectric constant of the sample deposited at 1.2 mbars as a function of the ac signal frequency. At low frequencies we found a high k value of 23, in agreement with the bulk value.[1] However, with increasing frequency the k value decreased, being 15 at 200 kHz. This decrease of the dielectric permittivity can be explained by the large density of point defects present in polycrystalline materials. Wagner and Sillars[36] proposed a model for the ac response of bulk dielectrics consisting of a perfect region and defective conducting regions. This model can be applied to our polycrystalline thin films by considering the grains as the perfect region and the boundaries as the defective regions. The two phases have different conductivities and dielectric constants and are modeled by two RC systems in series. The calculated dielectric constant of this system depends on the ac frequency signal, increasing with respect to the expected value of the perfect region for low frequencies and decreasing for high frequencies, as we observe for our films. This suggests that decreasing the defect content of the films (for instance, by means of postdeposition annealing) would lead to a stable, high k value of the HfO_2 films. It was also demonstrated that care must be taken when analyzing the dielectric permittivity of defective films if only C-V measurements performed at one single frequency are considered.

Although devices with film thickness in the range of nanometers have not been examined in this study, the unsatisfactory electrical properties obtained for these films reduce the application of HPRS HfO_2 in the field of the complementary MOS (CMOS) technology. Additionally, the polycrystalline structure and the high H content of the films lead to uniformity and reliability issues, ruling out this system in favor of other deposition techniques, for instance ALD, in which the uniformity and thickness control are not a cause of concern.

IV. CONCLUSION

The growth kinetics of the silicon oxide interfacial layer and the physical properties of HfO_2 deposited by HPRS using different deposition pressures and times have been reported. From the HI-ERDA measurements we observed a slightly oxygen rich stoichiometry and a high concentration of hydrogen due to high affinity for moisture of the HfO_2 films. Traces from other light elements such as B, C, N, and F were also detected. Several techniques have shown that the deposited HfO_2 films were polycrystalline, with a monoclinic structure. The influence of the deposition pressure on the grain size, the density, and the deposition rate of the HfO_2 films was studied. The HfO_2 growth rate decreased according to a power law when the deposition pressure increased, which is attributed to a decrease of the thermalization distance of the sputtered particles and to the less efficient process of transport of sputtered species through the plasma towards the substrate. The thickness of the interfacial SiO_2 layer showed a minimum for intermediate deposition pressures (about 1.2 mbars). It was also observed that the SiO_2 film grows mainly during the initial stages of the deposition process. Based on these results, we attribute the initial growth of the silicon oxide interface to the oxidation of the silicon surface, and the slower subsequent growth of the SiO_2 layer due to diffusion of oxygen through the grain boundaries of the HfO_2 film. Finally, we observed a frequency dependency of the k value in the 40 Hz–200 kHz range, which we attribute to the defective properties of the polycrystalline films. The SiO_2 interfacial layer formed during the sputtering process rules out the growth of high-k dielectrics on silicon by HPRS with small equivalent oxide thickness, unless some treatment of the Si surface is performed in order to prevent the growth of the SiO_2 layer.

However, the deposition rate obtained by HPRS and the HfO_2 properties such as refractive index, optical band gap, microstructure, and density found in this study make the films suitable for their application as transparent coatings and/or chemical inert layers.

ACKNOWLEDGMENTS

The authors acknowledge C.A.I. de Técnicas Físicas, C.A.I. de Espectroscopía y Espectrometría, and C.A.I. de Microscopía y Citometría of the Universidad Complutense de Madrid for technical support. J. Gandía and J. Cárabe (CIEMAT) are acknowledged for optical measurements. J.J. Jiménez (UCM) is gratefully acknowledged for careful discussion on sputtering system. This work was made possible thanks to the AP2003-4434-FPU grant of the Spanish M.E.C. and the contracts TEC 2004-1237/MIC and TEC2007/63318 of the the Spanish M.C.Y.T.

[1]J. Robertson, Rep. Prog. Phys. **69**, 327 (2006).
[2]S. H. Oh *et al.*, Digest of Technical Papers of the 2003 Symposium on VLSI Technology, 2003 (unpublished), pp. 73–74.
[3]M. Lesser, Opt. Eng. **26**, 911 (1987).
[4]M. Fadel, O. A. Azim, O. A. Omer, and R. R. Basily, Appl. Phys. A: Mater. Sci. Process. **66**, 335 (1998).
[5]C. Moldovan, R. Iosub, M. Modreanu, D. Ulieru, B. Firtat, and M. Ion, International Semiconductor Conference 2006 (unpublished), pp. 185–188.
[6]T. Wang, C. Chang, and J. G. Hwu, IEEE Sens. J. **6**, 1468 (2006).
[7]F. Wallrapp and P. Fromherz, J. Appl. Phys. **99**, 114103 (2006).
[8]H. Grüger, Ch. Kunath, E. Kurth, S. Sorge, W. Pufe, and T. Pechstein, Thin Solid Films **447–448**, 509 (2004).
[9]U. Poppe *et al.*, J. Appl. Phys. **71**, 5572 (1992).
[10]B. Chapman, *Glow Discharge Processes* (Wiley, New York, 1980).
[11]M. A. Navacerrada, M. L. Lucía, and F. Sánchez-Quesada, Phys. Rev. B **61**, 6422 (2000).
[12]E. San Andrés *et al.*, J. Vac. Sci. Technol. A **23**, 1523 (2005).
[13]M. I. Faley, S. B. Mi, A. Petraru, C. L. Jia, U. Poppe, and K. Urban, Appl. Phys. Lett. **89**, 082507 (2006).
[14]F. L. Martínez, M. Toledano, E. San Andrés, I. Mártil, G. González-Díaz, W. Bohne, J. Röhrich, and E. Strub, Thin Solid Films **515**, 695 (2006).
[15]W. Kern, RCA Rev. **31**, 187 (1970).
[16]W. Bohne, J. Röhrich, and G. Röschert, Nucl. Instrum. Methods Phys. Res. B **136–138**, 633 (1998).
[17]W. Bohne, S. Hessler, and G. Röschert, Nucl. Instrum. Methods Phys. Res. B **113**, 78 (1996).
[18]W. Bohne, W. Fuhs, J. Röhrich, B. Selle, G. González-Díaz, I. Mártil, F. L. Martínez, and A. del Prado, Surf. Interface Anal. **30**, 534 (2000).
[19]J. L. Hernández-Rojas, M. L. Lucía, I. Mártil, G. González-Díaz, J. Santamaría, and F. Sánchez-Quesada, Appl. Opt. **31**, 1606 (1992).
[20]J. Tauc, R. Grigorovici, and A. Vancu, Phys. Status Solidi **15**, 627 (1966).
[21]B. D. Cullity, *Elements of X-ray Diffraction* 2nd ed. (Addison-Wesley, Reading, MA, 1978).
[22]E. H. Nicollian and J. R. Brews, *MOS Physics and Technology* (Wiley, New York, 1982), p. 197.
[23]M. M. Frank, S. Sayan, S. Dörmann, T. J. Emge, L. S. Wielunski, E. Garfunkel, and Y. J. Chabal, Mater. Sci. Eng., B **109**, 6 (2004).
[24]D. A. Neumayer and E. Cartier, J. Appl. Phys. **90**, 1801 (2001).
[25]J. T. Fitch, S. S. Kim, and G. Lucovsky, J. Vac. Sci. Technol. A **8**, 1871 (1990).
[26]A. Kawamoto, J. Jameson, P. Griffin, K. Cho, and R. Dutton, IEEE Electron Device Lett. **22**, 14 (2001).
[27]M. Mayer, IPP Report No. 9/113, 1997 (unpublished).
[28]P. Raghu, N. Rana, C. Yim, E. Shero, and F. Shadman, J. Electrochem. Soc. **150**, F186 (2003).
[29]D. L. Wood, K. Nassau, T. Y. Kometani, and D. L. Nash, Appl. Opt. **29**, 604 (1990).
[30]R. E. Hann, P. R. Suitch, and J. L. Pentecost, J. Am. Ceram. Soc. **68**, 285 (1985).
[31]W. Umrath, *Fundamentals of Vacuum Technology. Leybold vacuum products and reference book 2001/2002* (Leybold, Cologne, 2001).
[32]I. Abril, A. Gras-Martí, J. J. Jiménez-Rodríguez, V. Konoplev, J. C. Moreno Marín, and A. M. C. Pérez-Martín, Trends in Vacuum Sci. & Tech. **1**, 251 (1993).
[33]A. G. Znamenski and V. A. Marchenko, Tech. Phys. **43**, 766 (1998).
[34]B. Tsui and H. Chang, J. Appl. Phys. **93**, 10119 (2003).
[35]K. J. Hubbard and D. G. Schlom, J. Mater. Res. **11**, 2757 (1996).
[36]W. D. Kingery, *Introduction to Ceramics* (Wiley, New York, 1960).
[37]L. Pantisano, J. Ramos, E. San Andrés-Serrano, Ph. J. Roussel, W. Sansen, and G. Groeseneken, Proceedings of the 2006 IEEE International Conference on Microelectronic Test Structures, 2006 (unpublished), pp. 222–225.